Article

Entropic Effects on Hydrated Alkali-Metal Cations: Infrared Spectroscopy and ab Initio Calculations of $M(HO)^-$ Cluster Ions for M = Li, Na, K, and Cs

Dorothy J. Miller, and James M. Lisy

J. Am. Chem. Soc., **2008**, 130 (46), 15393-15404 • DOI: 10.1021/ja803666m • Publication Date (Web): 22 October 2008

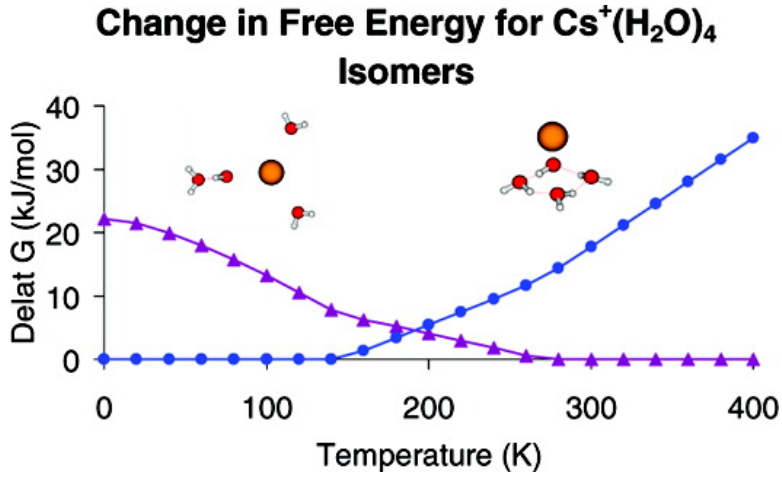

More About This Article

Additional resources and features associated with this article are available within the HTML version:

- Supporting Information
- Links to the 1 articles that cite this article, as of the time of this article download
- Access to high resolution figures
- Links to articles and content related to this article
- Copyright permission to reproduce figures and/or text from this article

View the Full Text HTML

J|A|C|S
ARTICLES

Published on Web 10/22/2008

Entropic Effects on Hydrated Alkali-Metal Cations: Infrared Spectroscopy and ab Initio Calculations of $M^+(H_2O)_{x=2-5}$ Cluster Ions for M = Li, Na, K, and Cs

Dorothy J. Miller and James M. Lisy*

Department of Chemistry, University of Illinois at Urbana−Champaign, Urbana, Illinois 6180

Received May 16, 2008; E-mail: j-lisy@uiuc.edu

Abstract: A delicate balance between competing and cooperating noncovalent interactions determines the three-dimensional structure of hydrated alkali-metal ion clusters. A critical factor influencing the balance reached is the internal energy content (or effective temperature) of the ion cluster. Cold cluster ions (~50−150 K) have little internal energy, and enthalpic contributions have a greater influence on the relative population of low-lying minima. In clusters whose internal energy distributions correspond to temperatures ~250−500 K, entropic effects are expected to influence which structural isomers are present, favoring those where free energy has been minimized. Infrared photodissociation spectra of $M^+(H_2O)_{x=2-5}$ (~250−500 K) are reported for M = Li, Na, K, and Cs to explore ion dependencies and entropic effects on the observed three-dimensional structure.

1. Introduction

The types of noncovalent interactions, specifically hydrogen bonding, observed in the immediate vicinity of a hydrated ion are the result of a balance between ion···water and water···water interactions. External factors, such as temperature, can greatly influence this balance of forces, lending stability to open structures with less extensive hydrogen bonding. As the temperature of the system increases, entropic effects have a greater impact on the free energy of the system. In order to investigate hydrated ions in real-world environments, it is important to study the relevant competing and cooperating noncovalent interactions in an appropriate model system: one capable of providing molecular-level details at temperatures roughly equivalent to ambient environments. Warm, gas-phase cluster ions are ideal systems to specifically probe molecular level noncovalent interactions in room-temperature systems.[1] As such, much theoretical[2−7] and experimental[8−21] effort has focused on understanding these simple model systems.

The type of noncovalent interaction(s) present in $M^+(H_2O)_x$ cluster ions can be explicitly probed using infrared vibrational spectroscopy in the OH stretching region. These stretching modes are particularly sensitive to their immediate environment, shifting in frequency in response to noncovalent perturbations.[15,22] The magnitude of the observed frequency shift is directly related to the strength of the perturbing noncovalent interaction, ranging from a few wavenumbers for weaker interactions to hundreds of wavenumbers for the strongest interactions. The electrostatic ion···water interaction weakens the water O—H covalent bonds, shifting both the symmetric and asymmetric OH stretching modes to lower frequency.[23−26] The strength of the alkali-metal ion···water interaction and, therefore, perturbation on the OH stretching modes is generally dependent on the charge density of the respective cation: $Li^+ > Na^+ > K^+ > Cs^+$.

Direct water···water interactions also shift the OH stretching modes. Formation of an O—H···O hydrogen bond weakens the O—H covalent bond in the proton-donating water molecule. This induces both a shift in OH stretching frequency and a significant increase in the infrared (IR) intensity of the hydrogen-bonded

(1) Cabarcos, O. M.; Weinheimer, C. J.; Lisy, J. M. *J. Phys. Chem. A* **1999**, *103*, 8777–8791.
(2) Lee, H. M.; Tarakeshwar, P.; Park, J.; Kolaski, M. R.; Yoon, Y. J.; Yi, H. B.; Kim, W. Y.; Kim, K. S. *J. Phys. Chem. A* **2004**, *108* (15), 2949–2958.
(3) Rajamani, S.; Ghosh, T.; Garde, S. *Biophys. J.* **2003**, *84* (2), 346A–346A.
(4) Rajamani, S.; Ghosh, T.; Garde, S. *J. Chem. Phys.* **2004**, *120* (9), 4457–4466.
(5) Schulz, F.; Hartke, B. *PCCP* **2003**, *5* (22), 5021–5030.
(6) Schulz, F.; Hartke, B. *Theor. Chem. Acc.* **2005**, *114* (4−5), 357–379.
(7) Varma, S.; Rempe, S. B. *Biophys. Chem.* **2006**, *124* (3), 192–199.
(8) Miller, D. J.; Lisy, J. M. *J. Am. Chem. Soc.* **2008**, *130*, 15381–15392.
(9) Castleman, A. W.; Bowen, K. H. *J. Phys. Chem.* **1996**, *100* (31), 12911–12944.
(10) Coe, J. V. *Int. Rev. Phys. Chem.* **2001**, *20* (1), 33–58.
(11) Duncan, M. A. *Annu. Rev. Phys. Chem.* **1997**, *48*, 69–93.
(12) Muller-Dethlefs, K.; Hobza, P. *Chem. Rev.* **2000**, *100* (1), 143–167.
(13) Kebarle, P. *Annu. Rev. Phys. Chem.* **1977**, *28*, 445–476.
(14) Stace, A. J. *PCCP* **2001**, *3*, 1935–1941.
(15) Bieske, E. J.; Dopfer, O. *Chem. Rev.* **2000**, *100* (11), 3963–3998.
(16) Buck, U.; Huisken, F. *Chem. Rev.* **2000**, *100* (11), 3863–3890.
(17) Duncan, M. A. *Int. J. Mass Spectrom.* **2000**, *200* (1−3), 545–569.
(18) Lisy, J. M. *Int. Rev. Phys. Chem.* **1997**, *16* (3), 267–289.
(19) Lisy, J. M. *J. Chem. Phys.* **2006**, (13), 125.
(20) Niedner-Schatteburg, G.; Bondybey, V. E. *Chem. Rev.* **2000**, *100* (11), 4059–4086.
(21) Robertson, W. H.; Johnson, M. A. *Annu. Rev. Phys. Chem.* **2003**, *54*, 173–213.
(22) Jeffrey, G. A. *An Introduction to Hydrogen Bonding*; Oxford University Press: New York, 1997; p 303.
(23) Vaden, T. D.; Forinash, B.; Lisy, J. M. *J. Chem. Phys.* **2002**, *117* (10), 4628–4631.
(24) Vaden, T. D.; Lisy, J. M.; Carnegie, P. D.; Pillai, E. D.; Duncan, M. A. *PCCP* **2006**, *8*, 3078–3082.
(25) Vaden, T. D.; Weinheimer, C. J.; Lisy, J. M. *J. Chem. Phys.* **2004**, *121* (7), 3102–3107.
(26) Bush, M. F.; Saykally, R. J.; Williams, E. R. *J. Am. Chem. Soc.* **2008**, *130* (28), 9122–9128.

OH feature relative to the non-hydrogen-bonded features.[12,27] The magnitude of the frequency shift caused by hydrogen bonding depends on the strength of the noncovalent interaction: stronger hydrogen bonds perturb the O—H covalent bonds more than weaker hydrogen bonds and, therefore, shift the respective OH stretching mode lower in frequency than weaker interactions. The cooperation between electrostatic and hydrogen-bonding interactions further perturbs the hydrogen-bonded OH oscillator. Such enhanced hydrogen bonds are shifted lower in frequency than the shift due to either hydrogen bonding or electrostatic perturbations individually. The efficiency of the hydrogen-bond enhancement is dependent on the ion···water interaction strength and hydrogen-bond angle.[14] The characteristic OH frequency shifts resulting from noncovalent perturbations often provide unambiguous evidence to the type and number of interactions present in $M^+(H_2O)_x$ ion clusters.

The balance between noncovalent interactions near 0 K may be different than the balance achieved at warmer temperatures, where entropic contributions to the available free energy increase. By varying source conditions, Lee and co-workers influenced the type of hydrogen bonds formed in $NH_4(H_2O)_5^+$ cluster ions.[28] The groups of Jordan and Johnson demonstrated a significant temperature dependency in the relative populations of hydrogen-bonded isomers observed in $I^-(CH_3OH)_n$ clusters.[29] Work from Kim and co-workers on hydrated alkali-metal cations suggests that global minimum energy isomers should be observed in cold cluster ions, while entropically driven isomers should be preferred at higher temperatures.[30] In recent collaboration between this group and Kim's group, the infrared photodissociation spectra of "cold" argon-tagged hydrated cesium ions were compared with theoretical (MP2/aug-cc-pVDZ) spectra of the minimum energy and low-lying isomers. There was general agreement between the zero-point-corrected energetic ordering of $Cs^+(H_2O)_{x=2-5}$ isomers and those identified in the $Cs^+(H_2O)_{x=2-5}Ar$ spectra.[31] However, there are significant discrepancies between this theoretical analysis and experimental observations when compared to the "warmer" $Cs^+(H_2O)_{x=1-5}$ spectra,[32] which had been previously reported by this group.

The significant difference between the $Cs^+(H_2O)_{x=1-5}$ and the $Cs^+(H_2O)_{x=2-5}Ar$ clusters is the internal energy content present in each system. Hydrated alkali-metal cluster ions formed in our laboratory stabilize solely through evaporation without collisional or three-body contributions. Over several successive evaporative events the internal energy content of the cluster ion decreases until the evaporation rate is slow compared with the time required to traverse our experimental apparatus ($\sim$200 μs). Therefore, the internal energy distributions must have an upper bound related to the binding energy of the most weakly bound ligand. Depending on the neutral expansion conditions, evaporative stabilization can occur via one of two paths: sequential evaporation of water molecules forming $M^+(H_2O)_x$ clusters or evaporation of argon atoms forming argon-tagged $M^+(H_2O)_xAr$ clusters. In the first path, evaporation of water, a significant amount of internal energy may remain after the cluster ion reaches a quasi-stable state due to the relatively high interaction energy of the evaporating water molecules with the cluster ion (+40 kJ/mol, vide infra). In the second path, evaporation of argon, each evaporative step removes a comparatively small amount of energy (the interaction energy of an argon atom with a $M^+(H_2O)_{x \geq 4}$ ion cluster, $\sim$3.8 kJ/mol, is significantly less than the water···cluster interaction),[8] but several additional evaporative events can occur. This ultimately results in a lower internal energy and a lower effective temperature in clusters formed by evaporation of argon than in those formed by water evaporation.

As illustrated above, the internal energy content of gas-phase clusters is inherently dependent upon the evaporative cooling pathway. The stabilization technique employed during formation has an equally important effect on the terminal internal energy content. A comparison of the experimental spectra and rotational temperatures of $Li^+(H_2O)_1Ar$ ion clusters formed either by evaporative cooling or by collisional cooling showed that these different stabilization techniques, while giving similar IR spectral features and therefore similar structures, generated cluster ions with substantially different internal energies.[24] Therefore, it is necessary to have a quantitative understanding of the effective cluster ion temperature when applying theoretical and experimental results as molecular-level descriptions of ion solvation.

2. Experimental Methods

The cluster ions studied in these experiments were generated and analyzed in the custom-built triple-quadrupole mass spectrometer that has been described elsewhere.[8] Briefly, the apparatus consists of three differentially pumped chambers: a source chamber, where ion clusters are formed; an ion guiding chamber, where ions evaporatively stabilize; and a detection chamber, where clusters are mass selected, photodissociated, and mass analyzed. In the source chamber, alkali-metal ions are generated by thermionic emission from a resistively heated tungsten filament coated with an alkali/halide-salt-impregnated paste. Neutral clusters are generated by a supersonic expansion of H_2O vapor in an argon carrier gas through a 180 μm diameter conical nozzle (backing pressure near 300 Torr) and perpendicularly intersected, approximately 30 mm downstream from the nozzle source, by the ion beam. Resulting cluster ions have approximately 10 eV of excess internal energy (from the collision and subsequent hydration) that is dissipated by water evaporation.

Nascent cluster ions are guided from the source chamber through a 1 mm skimmer into the ion guiding chamber, where a set of electrostatic lenses guides the ions as they lose both mass and internal energy over several evaporative steps. The quasi-stable ion clusters are then introduced into the detection chamber, where the species of interest are mass selected and photodissociated following absorption of a single photon from one of two tunable infrared lasers counter propagating along the axis of the experimental apparatus ($LiNbO_3$ optical parametric oscillator pumped by a 20 Hz Nd:YAG or LaserVision OPO/OPA pumped by a 10 Hz Surelite II). The remaining parent cluster ions and resulting ion fragments are mass analyzed to determine the extent of dissociation by recording the percent fragmentation as a function of IR frequency. This is reported as the predissociation cross section by correcting for the laser fluence. Absolute frequency calibration is achieved by concurrently acquiring the photoacoustic spectrum of ambient atmospheric water vapor. Reported infrared photodissociation (IRPD) spectra have been smoothed with a three-point-adjacent-averaging algorithm.

(27) Kozmutza, C.; Varga, I.; Udvardi, L. *J. Mol. Struct.* **2003**, *666−667*, 95–97.
(28) Chang, H. C.; Wang, Y. S.; Lee, Y. T.; Chang, H. C. *Int. J. Mass Spectrom.* **1998**, *179/180*, 91–102.
(29) Robertson, W. H.; Karapetian, K.; Ayotte, P.; Jordan, K. D.; Johnson, M. A. *J. Chem. Phys.* **2002**, *116* (12), 4853–4857.
(30) Kim, J. S.; Lee, S.; Cho, S. J.; Mhin, B. J.; Kim, K. S. *J. Chem. Phys.* **1995**, *102* (2), 839–849.
(31) Kolaski, M.; Lee, H. M.; Choi, Y. C.; Kim, K. S.; Tarakeshwar, P.; Miller, D. J.; Lisy, J. M. *J. Chem. Phys.* **2007**, (7), 126.
(32) Weinheimer, C. J.; Lisy, J. M. *J. Chem. Phys.* **1996**, *105* (7), 2938–2941.

3. Theoretical Calculations

3.1. Ab Initio Calculations. Preliminary $M^+(H_2O)_x$ structures were generated with Spartan 02[33] using a molecular mechanics geometry optimization with the Merck Molecular Force Field and/or an in-house Monte Carlo simulated annealing algorithm.[34] Energies and frequencies were then calculated using the GAUSSIAN 03 software package.[35] Oxygen, hydrogen, and argon atoms as well as the lithium and sodium cations were treated with the augmented-correlation-consistent all-electron basis set, aug-cc-pVDZ. The larger potassium and cesium cations were treated with the Los Alamos double-ζ basis with effective core potentials.[36−38] Geometry optimization and frequency calculations were evaluated with second-order Møller−Plesset (MP2) theory to accommodate dispersive interactions, which are important when calculating binary interactions involving cations.[12] Basis-set superposition error was neglected, as basis-set error minimally impacts relative energy differences.[39] Theoretical spectra were generated using SWizard[40] with an average Gaussian peak width of 20 cm^{-1} and scaled by 0.9604[41] to facilitate comparison with experimental data.

3.2. Internal Energy and Temperature Approximations. The internal energies and, therefore, effective temperatures of our cluster ions were modeled using the Rice−Ramsperger−Kassel--Marcus evaporative ensemble (RRKM-EE) formulism.[1] Cluster ion internal energy (IE) distributions were modeled by calculating the unimolecular dissociation rates for each cluster as a function of IE and then, assuming the evaporative ensemble formulism, propagated for the time required to completely traverse the detection chamber of our experimental apparatus. Clusters formed by evaporation of water molecules were assumed to originate from larger $M^+(H_2O)_x$ clusters. IE distributions and average temperatures for these systems were simulated from an ensemble of $M^+(H_2O)_x$ species with $x \leq 4$. Argon-tagged cluster ions were assumed to form from larger $M^+(H_2O)_xAr_y$ clusters through the sequential evaporative loss of argon atoms. Therefore, IE distributions and average temperatures for these species were simulated from an ensemble of $M^+(H_2O)_xAr_y$ clusters where $y \leq 4$ to allow for evaporative cooling.

The internal energies of our cluster ions were modeled using the evaporative ensemble[1,42,43]

$$F(t) = \frac{\int P_{n-1}(\mathrm{IE}, t)\, \mathrm{d}IE}{\int P_{n-1}(\mathrm{IE}, t)\, \mathrm{dIE} + \int P_n(IE, t)\mathrm{dIE}} \tag{3.1}$$

where P_{n-1}(IE,t) and P_n(IE,t) are the respective population distributions of the parent and fragment cluster ions as a function of IE at time t and $F(T)$ is the fraction dissociated. In this method, P(IE,t) is propagated for a time corresponding to the experimental ion time-of-flight through the detection chamber. The time scale of our experiment ($\sim$200 μs) ensures that the internal energy of a cluster ion has been distributed evenly through the available degrees of freedom. The evaporation rates as a function of internal energy, k(IE), were calculated from the usual RRKM relation[44−46]

$$k(\mathrm{IE}) = \left(\frac{Q^{\ddagger}}{Q}\right)\frac{DW^{\ddagger}(\mathrm{IE}^{\ddagger})}{h\rho(\mathrm{IE})} \tag{3.2}$$

where $IE^{\ddagger}$ is the total internal energy minus the cluster···evaporating-ligand binding energy (BE), h is Plank's constant, $(Q^{\ddagger}/Q)$ is the ratio of rotational partition functions of the transition state to the energized molecule and accounts for the rotational contribution to the RRKM rate, D is the degeneracy of transition states and was assumed to be the number of identical evaporating ligands present in the parent cluster, ρ(IE) is the vibrational density of states and was determined by taking the derivative of the sum of states with respect to energy, and $W^{\ddagger}$ is the transition-state vibrational sum of states and was calculated using the Beyer−Swinehart algorithm[47,48] with vibrational frequencies obtained from ab initio calculations (details above). $(Q^{\ddagger}/Q)$ was calculated from[49]

$$\left(\frac{Q^{\ddagger}}{Q}\right) = \sqrt{\left(\frac{\alpha e^2}{8\varepsilon_0 r_e^4 k_B T}\right)} \tag{3.3}$$

where α is the polarizability of the evaporating ligand (1.64×10^{-24} cm^3 for argon and 1.45×10^{-24} cm^3 for water),[50] r_e is the equilibrium distance between the evaporating ligand and the remaining cluster ion, e is the elementary charge constant, ε_0 is the vacuum permittivity constant, k_B is the Boltzman constant, and T is the temperature. Vibrational frequencies, BE's, and r_e's were obtained from ab initio calculations (details specified above).

The internal energy distribution coupled with the ab initio vibrational frequencies and RRKM rate are then used to extrapolate a cluster temperature using the following relations[1]

$$\mathrm{IE}_{vr}(T) = \sum_{j=1}^{m} E_{vj}(T) + IE_r(T) \tag{3.4}$$

where $IE_{vr}(T)$ is the total internal energy, $IE_r(T) = (3/2)k_BT$ is the rotational energy component to the internal energy, and IE_{vj} is the vibrational contribution to the IE from the jth vibrational mode and is represented by

$$\mathrm{IE}_{vj} = \frac{k_B\Theta_{vj}e^{\Theta_{vj}/T}}{(1-e^{\Theta_{vj}/T})} \text{ with } \Theta_{vj} = \frac{h\nu_j}{k_B} \tag{3.5}$$

The temperature of the cluster ion ensemble is then calculated at cluster propagation time equivalent to the entrance, midpoint, and exit of the second quadrupole and then averaged to estimate a temperature for each cluster ion.

The molecular partition function, $Q(T)$, was computed for the $M^+(H_2O)_x$ clusters from ab initio harmonic vibrational frequencies and ZPE-corrected energies using the thermo.pl PERL script.[51] Finally, the change in Gibbs free energy, $G(T)$, for the $M^+(H_2O)_x$ clusters was evaluated for $T = 0-400$ K.

4. Results and Discussion

Prior to photodissociation, $M^+(H_2O)_x$ clusters have an elevated amount of inherent internal energy. This internal energy content allows multiple structural isomers to be simultaneously present in the molecular beam and gives rise to multiple spectral features with comparable IR intensity. By adjusting the expansion conditions (higher backing pressure and lower partial

(33) Deppmeier, B. J. *SPARTAN'02*, SPARTAN 2002 SGI IRIX 64 (mips4); Wavefunction, Inc.: Irvine, CA, 2002.
(34) Nicely, A. *Ion Cluster Structure Generator 06*; Department of Chemistry, University of Illinois: Urbana, IL, 2007.
(35) Frisch, M. J. *Gaussian 03*, B.04; Gaussian: Pittsburgh, PA, 2003.
(36) Hay, P. J.; Wadt, W. R. *J. Chem. Phys.* **1985**, *82* (1), 270–283.
(37) Hay, P. J.; Wadt, W. R. *J. Chem. Phys.* **1985**, *82* (1), 299–310.
(38) Wadt, W. R.; Hay, P. J. *J. Chem. Phys.* **1985**, *82* (1), 284–298.
(39) Lee, H. M.; Kim, J.; Lee, S.; Mhin, B. J.; Kim, K. S. *J. Chem. Phys.* **1999**, *111* (9), 3995–4004.
(40) Gorelsky, S. I. *SWizard program, 4.1*; Centre for Catalysis Research and Innovation, University of Ottawa: Ottawa, Canada, 2005.
(41) Sinha, P.; Boesch, S. E.; Gu, C.; Wheeler, R. A.; Wilson, A. K. *J. Phys. Chem. A* **2004**, *108* (42), 9213.
(42) Klots, C. E. *Nature* **1987**, *327*, 222–223.
(43) Klots, C. E. *J. Chem. Phys.* **1985**, *83* (11), 5854–5860.
(44) Rice, O. K.; Ramsperger, H. C. *J. Am. Chem. Soc.* **1927**, *49* (7), 1617–1629.
(45) Kassel, L. S. *J. Phys. Chem.* **1928**, *32* (2), 225–242.
(46) Marcus, R. A. *J. Chem. Phys.* **1951**, *20* (3), 359–364.
(47) Beyer, T.; Swinehar, D. F. *Commun. Acm* **1973**, *16* (6), 379–379.
(48) Stein, S. E.; Rabinovi, B. S. *J. Chem. Phys.* **1973**, *58* (6), 2438–2445.
(49) Rodgers, M. T.; Ervin, K. M.; Armentrout, P. B. *J. Chem. Phys.* **1997**, *106* (11), 4499–4508.
(50) Lide, D. R. *CRC Handbook of Chemistry and Physics Internet Version 2007*, 87th ed.; Taylor and Francis: Boca Raton, FL, 2006−2007.
(51) Irikura, K. K. *THERMO.PL*; Chemical Science and Technology Laboratory, National Institute of Standards and Technology: Gaithersburg, MD, 2002.

Table 1. Interaction Energies (kJ/mol) for the $M^+(H_2O)_{1-2}$ Cluster Constituents

	theoretical[a] ΔE_E	experimental ΔE_0	ΔH°
$Li^+\cdots(H_2O)$	−137.2	−129.2	−142.3[b]
$Li^+(H_2O)_1\cdots(H_2O)_1$	−123.0	−114.4	−108.0[b]
$Na^+\cdots(H_2O)$	−93.1	−87.1	−100.4[b]
$Na^+(H_2O)_1\cdots(H_2O)_1$	−85.1	−79.0	−82.8[b]
$K^+\cdots(H_2O)$	−63.6	−58.5	−74.9[c]
$K^+(H_2O)_1\cdots(H_2O)_1$	−60.3	−55.2	−67.4[c]
$Cs^+\cdots(H_2O)$	−47.8	−43.4	−57.3[b]
$Cs^+(H_2O)_1\cdots(H_2O)_1$	−45.4	−40.9	−52.3[b]

[a] This work. [b] References 13 and 52. On the basis of reaction equilibrium constants. [c] References 13, 52, and 53. On the basis of reaction equilibrium constants.

pressure of water vapor), neutral clusters comprised with large numbers of argon atoms are formed. After collision with the alkali-metal ions $M^+(H_2O)_xAr$ clusters are formed primarily by evaporation of argon atoms instead of evaporation of water molecules. These clusters have reduced internal energy compared with the warmer $M^+(H_2O)_x$ species and, therefore, have less congested IRPD spectra: typically, the cold $M^+(H_2O)_{x\leq4}Ar$ spectra had features attributable to a single isomer.[8] Therefore, where needed, the previously reported spectra of cold $M^+(H_2O)_xAr$ (M = Li, Na, K, and Cs) cluster ions will serve as a basis for comparison when identifying contributing isomers to the warmer $M^+(H_2O)_x$ spectra.

4.1.$M^+(H_2O)_1$. Typical ion···water binding energies, reported in Table 1, are greater than the energy of a single IR photon, which prevents direct acquisition of the $M^+(H_2O)_1$ IRPD spectra. However, the OH frequency shifts induced by complexation with an alkali-metal cation have been previously reported for the $M^+(H_2O)_1Ar$ (M = Li, Na, K, and Cs) cluster ions.[23−25] These spectra provide a basis for interpreting the OH frequency shifts arising solely from electrostatic perturbations. OH stretching frequencies and assignments for the $M^+(H_2O)_x$ cluster constituents are listed in Table 2. There, the electrostatic ion···dipole interaction shifted the associated OH stretching modes lower in frequency relative to their counterparts in neutral water monomer.

4.2. $M^+(H_2O)_2$. In the $M^+(H_2O)_2$ (M = Na, K, and Cs) cluster ions a reduction in the pairwise ion···water interaction energies facilitates some cluster fragmentation after absorption of a single IR photon. The electrostatic interactions present in the $Li^+(H_2O)_2$ clusters (see Table 1), however, are still too great to permit single-photon dissociation.

Two features are present in the $M^+(H_2O)_2$ (M = K and Cs) spectra: a relatively narrow band near 3630 cm^{-1} and a much broader band roughly centered near 3740 cm^{-1}, which are shown in Figure 1. These bands can be straightforwardly assigned to the symmetric and asymmetric OH stretching modes by comparison with the previously reported $M^+(H_2O)_2Ar$ spectra.[8] The symmetric OH stretch is a parallel vibrational transition, while the asymmetric band is a perpendicular transition with $\Delta K = \pm1$ rotational substructure. The spectrum of $Na^+(H_2O)_2$ is also given. However, due to the higher binding energy and corresponding higher temperature, this system is at the limits of detection and will not be further analyzed. The calculated minimum-energy structure of the $M^+(H_2O)_2$ clusters, depicted in Figure 2, shows that these dihydrated species assume a linear conformation with the cation in the center and the water molecules, dipole oriented toward the ion, located on either end and able to freely rotate about their symmetry axis. The asymmetric OH stretch is a perpendicular transition with $\Delta K = \pm1$ selection rules. With a substantial K state population distribution at the observed temperatures, this will give rise to

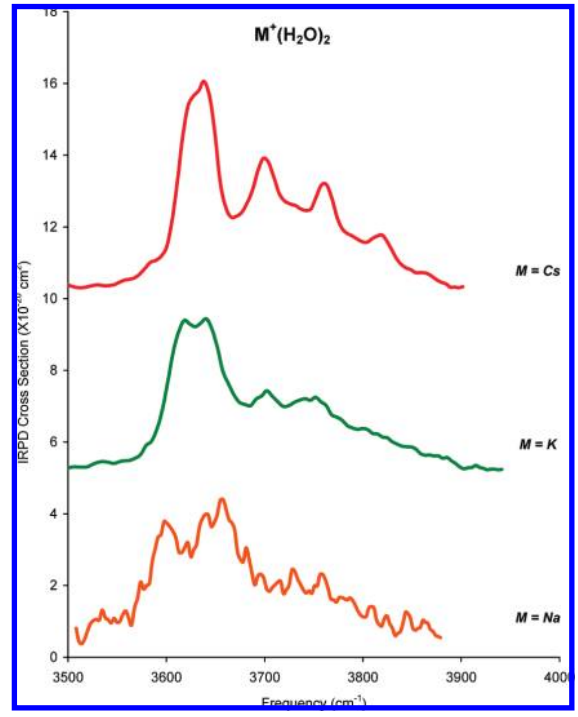

Figure 1. $M^+(H_2O)_2$ IRPD spectra for M = Na, K, and Cs in the free OH stretching region.

Table 2. Observed OH Stretching Vibrations for $(H_2O)_{1-5}$ and $M^+(H_2O)_x$ with Their Assignments

cluster	frequency (cm^{-1})	mode	cluster	frequency (cm^{-1})	mode
H_2O[54,55]	3755.97	asym	$(H_2O)_4$[56−58]	3720	free
	3657.05	sym		3416	HB, cyclic
$Li^+(H_2O)_1Ar$[24]	3696	asym	$Li^+(H_2O)_4$	3723.9	asym
	3631	sym		3645.5	sym
$Na^+(H_2O)_1Ar$[25]	3707.0	asym	$Na^+(H_2O)_4$	3734.4	asym
	3634.5	sym		3644.3	sym
$K^+(H_2O)_1Ar$[25]	3710.0	asym		3418.5	HB, linear
	3636.0	sym	$K^+(H_2O)_4$	3723.0	asym
$Cs^+(H_2O)_1Ar$[23,25]	3711.5	asym		3640.1	sym
	3635.4	sym		3562.0	HB, bent
$(H_2O)_2$[56−60]	3715	asym		3460.3	HB, linear
	3698	free	$Cs^+(H_2O)_4$	3709.9	asym/free
	3627	sym		3638.3	sym
	3550	HB, linear		3559.8	HB, bent
$Li^+(H_2O)_2$	N/A	asym		3473.5	HB, linear
	N/A	sym	$(H_2O)_5$[56−58]	3720	free
$Na^+(H_2O)_2$	N/A	asym		3360	HB, cyclic
	N/A	sym	$Li^+(H_2O)_5$	3718.1	asym/free
$K^+(H_2O)_2$	3740	asym		3651.5	sym
	3630	sym		3549.8	HB, bent
$Cs^+(H_2O)_2$	3730	asym		3427.3	HB, linear
	3630	sym	$Na^+(H_2O)_5$	3719.0	asym/free
$(H_2O)_3$[56−58]	3726	free		3646.5	sym
	3533	HB, cyclic		3558.9	HB, bent
$Li^+(H_2O)_3$	3755.1	asym		3455.3	HB, linear
	3636.0	sym	$K^+(H_2O)_5$	3713.5	asym/free
$Na^+(H_2O)_3$	3754.4	asym		3642.4	sym
	3640.0	sym		3565.1	HB, bent
$K^+(H_2O)_3$	3736.4	asym		3472.6	HB, linear
	3637.8	sym	$Cs^+(H_2O)_5$	3706.9	asym/free
$Cs^+(H_2O)_3$	3713.8	asym/free		3641.8	sym
	3637.7	sym		3571.1	HB, bent
	3548.7	HB, bent		3488.6	HB, linear
	3460.5	HB, linear		3410.1	HB, cyclic

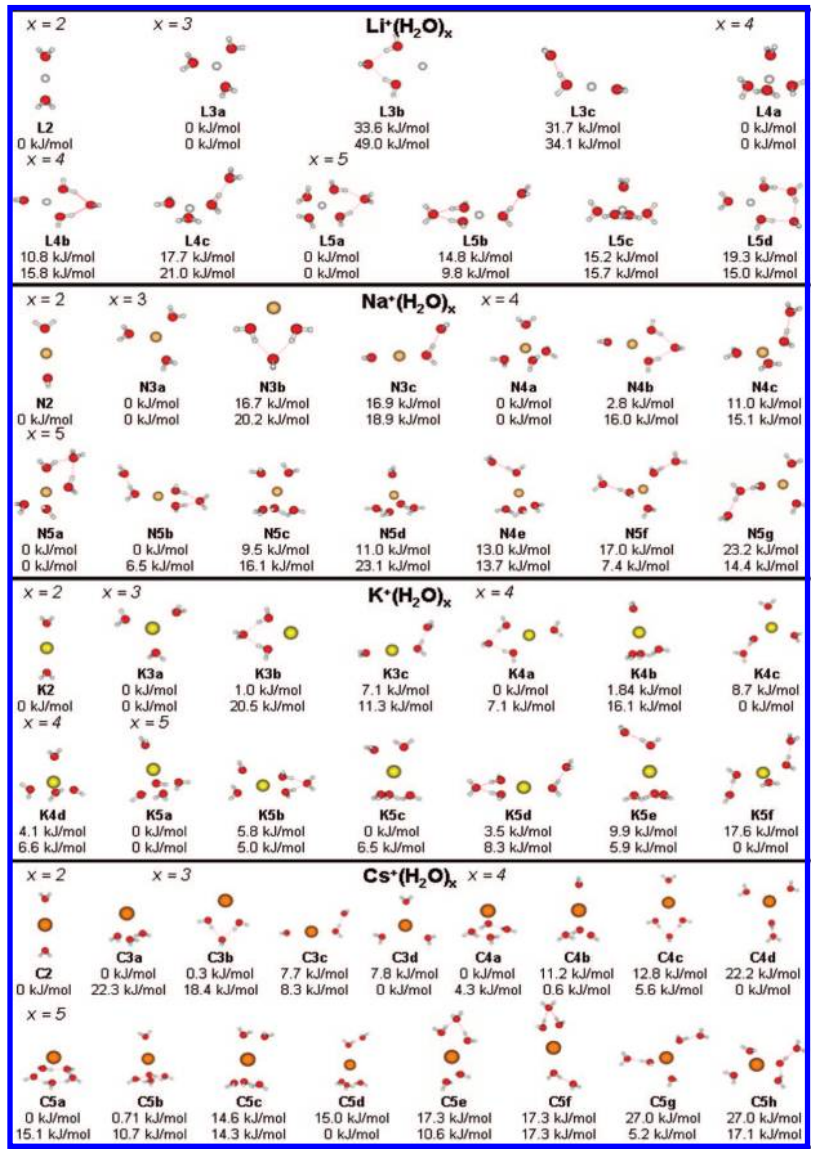

Figure 2. Low-lying structures for $M^+(H_2O)_x$ for M = Li, Na, K, and Cs and $x = 2-5$. The first letter in the structure label reflects the ion. The number corresponds with the number of water molecules present in the cluster. The lower case letter indicates the relative energy ordering of that isomer (a < b < c, etc.). Relative energies (in kJ/mol) are reported at 0 K, top, and at the RRKM-EE estimated temperature (see Table 3), bottom. Estimated RRKM-EE temperatures for the $x = 4$ clusters were used for the $x = 5$ clusters.

the breath and partial rotational structure associated with this band. The symmetric stretch is a parallel transition with $\Delta K = 0$ selection rules and has a more compact band structure. As the binding energies decrease (Na^+ to Cs^+), so does the effective temperature, which in turn leads to more resolvable features. Thermal broadening is a constant contributor to the width of the OH features. RRKM-EE cluster temperatures for the $M^+(H_2O)_x$ clusters and, for comparison, the $M^+(H_2O)_2Ar$ systems are listed in Table 3.

4.3. $M^+(H_2O)_3$. Spectra for the smaller $M^+(H_2O)_3$ (M = Li, Na, and K) clusters, shown in Figure 3, are very similar. Two OH stretching features, near 3735 and 3640 cm^{-1}, are observed. Like in the $M^+(H_2O)_2$ clusters, these features are associated with the asymmetric and symmetric OH stretching modes, respectively. Both thermal and rotational broadening are again observed in the $M^+(H_2O)_3$ spectra; however, unlike the $M^+(H_2O)_2$ systems, Li^+ and Na^+ have assignable symmetric stretch features. These differences come from several factors: the binding energy for the next evaporative step is lower, resulting in a lower internal energy and lower cluster temperatures (listed in Table 3); more of the $M^+(H_2O)_3$ clusters generated fragment after absorption of a single IR photon; and there are more contributing OH oscillators per transition.

Table 3. RRKM-EE Estimated Temperatures for $M^+(H_2O)_2Ar$ and $M^+(H_2O)_{2-4}$ Cluster Ions

cluster	*T* (K)	cluster	*T* (K)
$Li^+(H_2O)_2Ar$	110	$K^+(H_2O)_2Ar$	50
$Li^+(H_2O)_2$	780	$K^+(H_2O)_2$	420
$Li^+(H_2O)_3$	485	$K^+(H_2O)_3$	300
$Li^+(H_2O)_4$	325	$K^+(H_2O)_4$	270
$Na^+(H_2O)_2Ar$	75	$Cs^+(H_2O)_2Ar$	40
$Na^+(H_2O)_2$	565	$Cs^+(H_2O)_2$	310
$Na^+(H_2O)_3$	385	$Cs^+(H_2O)_3$	300
$Na^+(H_2O)_4$	305	$Cs^+(H_2O)_4$	270

In the $Cs^+(H_2O)_3$ spectrum (Figure 3) two additional features are observed near 3550 and 3460 cm^{-1}. These weak features are observed in the spectral region (below 3600 cm^{-1}) traditionally associated with water···water hydrogen bonding and

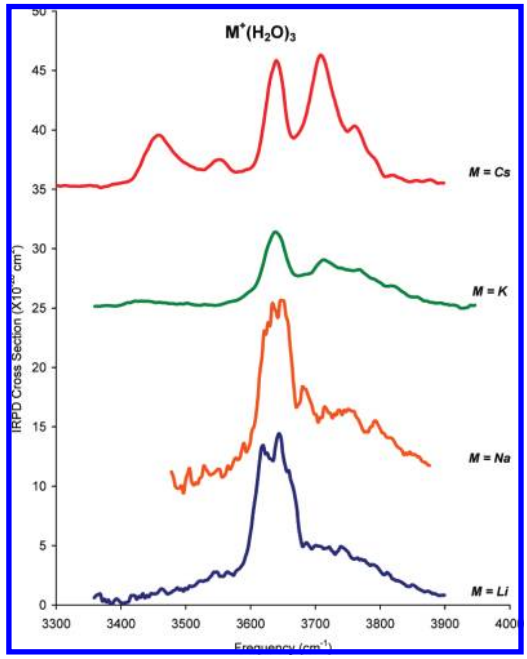

Figure 3. $M^+(H_2O)_3$ IRPD spectra for M = Li, Na, K, and Cs in the free and hydrogen-bonded OH stretching regions.

indicate that such interactions are present. As discussed earlier, hydrogen-bond formation causes a shift to lower frequency of the hydrogen-bonded OH stretch as well as an increase in the relative intensity of that feature relative to the non-hydrogen-bonded symmetric OH feature (3637 cm^{-1}). In the $Cs^+(H_2O)_3$ spectrum both of the hydrogen-bonded features, while clearly present, are less intense than the symmetric band near 3637 cm^{-1}, which suggests that direct water···water interactions are not extensive for this size and composition. A significant number of the $Cs^+(H_2O)_3$ clusters have no water···water hydrogen bonds.

To assist in identifying the water···water interactions present, several low-lying structures were optimized, three of which possessed distinct types of water···water interactions: bent, linear, and cyclic water···water hydrogen bonding, as shown in Figure 2. Briefly, bent hydrogen bonds are formed when two first-shell water molecules, acting as proton donors, interact with a single proton-accepting water molecule in the second shell (C3b). Linear hydrogen bonds occur when a first-shell proton-donating water molecule forms a hydrogen bond with a second-shell proton-accepting water molecule (C3c). Cyclic hydrogen bonds form when each water molecule acts as both a proton donor and a proton acceptor (C3a). The ZPE ordering of the low-lying $Cs^+(H_2O)_3$ isomers (spectra and structures shown in Figure 4) indicates that the C3a and the C3b conformations are nearly isoenergetic while the non-hydrogen-bonded, C3d, isomer is ~7.5 kJ/mol higher in energy. This suggests that a hydrogen-bonded OH feature—whether from the isomer containing bent hydrogen bonds or the isomer with cyclic water···water hydrogen bonding—should be the most IR intense transition present. In addition, in the colder $Cs^+(H_2O)_3Ar$ clusters,[8] a cyclic water···water hydrogen-bonded signature was observed. However, this interpretation does not agree with the experimental features observed in the $Cs^+(H_2O)_3$ spectrum, where non-hydrogen-bonded OH vibrations are the most intense features present.

RRKM-EE temperature estimates of $Cs^+(H_2O)_3$ cluster ions (Table 3) indicate that these clusters are expected to be much warmer than 0 K. Therefore, an analysis of the energetic ordering of the $Cs^+(H_2O)_3$ clusters near the estimated temperature of 300 K should more accurately represent the population of isomers present in the molecular beam. The change in free energy as a function of energy for the four low-lying $Cs^+(H_2O)_3$ is shown in Figure 5. Clearly, as the temperature increases, isomers with more hydrogen bonding, such as those containing bent or cyclic water···water hydrogen bonding, become increasingly unstable while those with fewer water···water hydrogen bonds (and, therefore, with less hindered water rotations) become more stable. Near 100 K, the low-lying isomers reorder, and by 300 K the non-hydrogen-bonded, C3d isomer is predicted to be the most energetically stable isomer, with the C3c (8.3 kJ/mol), C3b (18.4 kJ/mol), and C3a (22.3 kJ/mol) hydrogen-bonded isomers located higher in free energy. This interpretation of the preferred low-lying structures is in much better agreement with the experimental spectrum and allows the hydrogen-bonded features observed to be straightforwardly assigned: a convolution of bent and cyclic water···water hydrogen bonding gives rise to the feature near 3550 cm^{-1}, while the slightly more intense hydrogen-bonded feature, near 3460 cm^{-1}, comes from linear water···water hydrogen bonding.

4.4. $M^+(H_2O)_4$. With more water molecules hydrating the ion, water···water hydrogen bonding is expected to become more energetically favorable. However, such water···water interactions are still not observed in the $Li^+(H_2O)_4$ spectrum, which is shown in Figure 6. The only features observed come from the non-hydrogen-bonded symmetric (3645 cm^{-1}) and asymmetric (3724 cm^{-1}) vibrations. This indicates that pairwise ion···water interactions in this cluster are still greater than the water···water interactions: a manifestation of the strong electrostatic interactions present in these cluster ions.

Electrostatic interactions are slightly reduced in the $Na^+(H_2O)_4$ spectrum due to a reduced charge density in the sodium-containing cluster ions, and a weak hydrogen-bonded feature near 3418 cm^{-1} is observed in addition to the non-hydrogen-bonded OH vibrations at 3734 (asymmetric) and 3644 cm^{-1} (symmetric). The hydrogen-bonded feature is within 42 cm^{-1} of the feature attributed to linear water···water hydrogen bonding in the $Cs^+(H_2O)_3$ spectrum. This similarity allows a straightforward assignment of the weak hydrogen-bonded feature near (3418 cm^{-1}) in the $Na^+(H_2O)_4$ spectrum to a linear water···water hydrogen bonding. The linear water···water hydrogen-bonded OH vibration in the $Cs^+(H_2O)_3$ spectrum (3460 cm^{-1}) is 42 cm^{-1} higher in frequency than the feature in the $Na^+(H_2O)_4$ cluster because, even though an additional ligand is present in the sodium containing cluster, the linear hydrogen bond is more strongly enhanced by the sodium cation than the cesium cation. This observation is supported by the ab initio

(52) Dzidic, I.; Kebarle, P. *J. Phys. Chem.* **1969**, *74* (7), 1466–1474.
(53) Searles, S.; Kebarle, P. *Can. J. Chem.* **1969**, *47*, 2619–2627.
(54) Fraley, P. E.; Rao, K. N. *J. Mol. Spectrosc.* **1969**, *29* (1−3), 312–347.
(55) Herzberg, G. *Molecular Spectra and Molecular Structure II. Infrared and Raman Spectra of Polyatomic Molecules*; Van Nostrand Reinhold: New York, 1945.
(56) Coker, D. F.; Miller, R. E.; Watts, R. O. *J. Chem. Phys.* **1985**, *82* (8), 3554–3562.
(57) Huisken, F.; Kaloudis, M.; Kulcke, A. *J. Chem. Phys.* **1996**, *104* (1), 17–25.
(58) Vernon, M. F.; Lisy, J. M.; Krajnovich, D. J.; Tramer, A.; Kwok, H. S.; Shen, Y. R.; Lee, Y. T. *Faraday Discuss.* **1982**, 387–397.
(59) Huang, Z. S.; Miller, R. E. *J. Chem. Phys.* **1989**, *91* (11), 6613–6631.
(60) Page, R. H.; Frey, J. G.; Shen, Y. R.; Lee, Y. T. *Chem. Phys. Lett.* **1984**, *106* (5), 373–376.

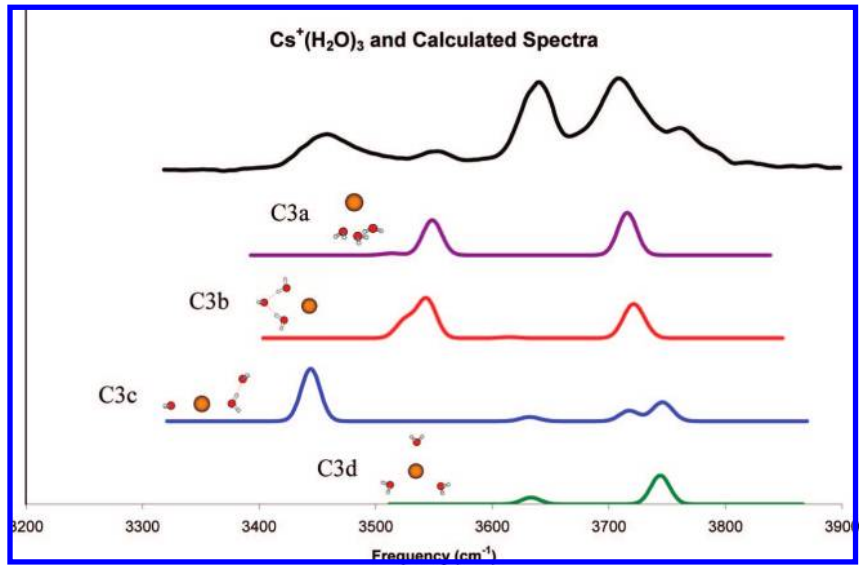

Figure 4. Experimental (top trace) and theoretical (lower traces) spectra of $Cs^+(H_2O)_3$. Theoretical spectra are ordered based on relative free energies at the RRKM-EE-estimated temperatures from most energetically stable to least energetically stable (bottom to top).

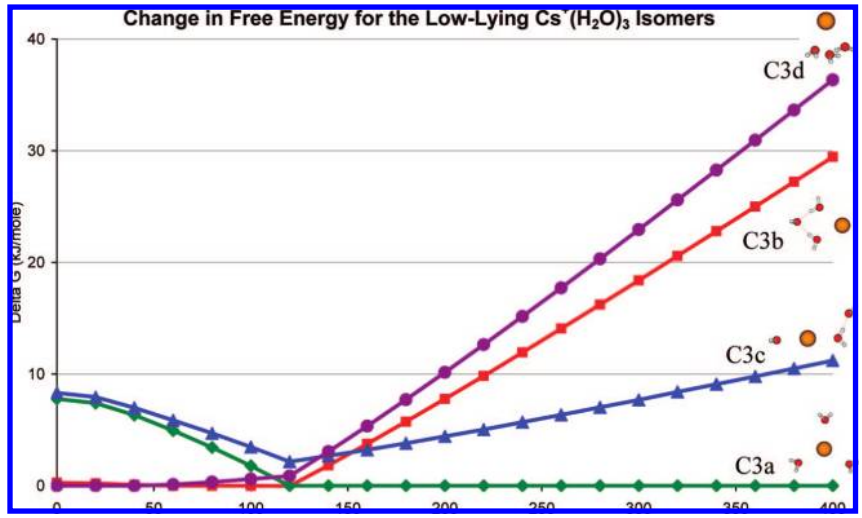

Figure 5. Change in free energy with respect to temperature (0−400 K) for the low-lying $Cs^+(H_2O)_3$ isomers: C3d, C3c, C3b, C3a.

calculations, which predict the hydrogen-bonded OH stretch for $Cs^+(H_2O)_3$ to be 53 cm^{-1} to higher frequency that the corresponding hydrogen-bonded mode in $Na^+(H_2O)_4$.

However, like in the $Cs^+(H_2O)_3$ system, the relative IR intensities of the hydrogen-bonded features are weaker than the much more intense symmetric OH stretch, indicating that the majority of $Na^+(H_2O)_4$ clusters assume a non-hydrogen-bonded, tetrahedral configuration (N4a in Figure 2). This is the calculated minimum energy $Na^+(H_2O)_4$ isomer at all temperatures evaluated. At 0 K, the bent hydrogen bond N4b isomer is only a few kJ/mol (2.8 kJ/mol) higher in energy than the N4a isomer while the linear hydrogen bond N4c isomer is ∼11 kJ/mol higher in energy than the minimum-energy N4a conformation. In the cold $Na^+(H_2O)_4Ar$ spectrum[8] the bent hydrogen-bonding motif was observed. As the temperature of the cluster increases however, the N4b isomer becomes increasingly less stable and near 280 K the energetic ordering of the N4b and N4c isomers invert, as shown in Figure 7. The RRKM-EE estimation of the internal energy content of the $Na^+(H_2O)_4$ clusters places the temperature of near 305 K, a temperature where the energetic ordering of the low-lying isomers is in good agreement with the IRPD spectrum.

Similar arguments may be put forward when assigning the weak hydrogen-bonded features in the $K^+(H_2O)_4$ spectrum, which is also shown in Figure 6. The hydrogen-bonded signatures present in the $K^+(H_2O)_4$ spectrum are very similar to those observed in the $Cs^+(H_2O)_3$ spectrum, shown in Figure 3, and assigned accordingly: the feature near 3460 cm^{-1} arises from a linear water···water hydrogen bond, while the feature near 3562 cm^{-1} is assigned to bent water···water hydrogen bonding. An isomer with cyclic water···water hydrogen bonding was not located for the $K^+(H_2O)_4$, allowing the feature near 3562 cm^{-1} to be exclusively assigned to bent water···water hydrogen bonding (minimum-energy isomers of $K^+(H_2O)_4$ are shown in Figure 2).

Because the electrostatic interactions present in the potassium-containing clusters are weaker than those in the sodium-containing clusters, the $K^+(H_2O)_4$ cluster is expected to have reduced internal energy compared with the $Na^+(H_2O)_4$ system.

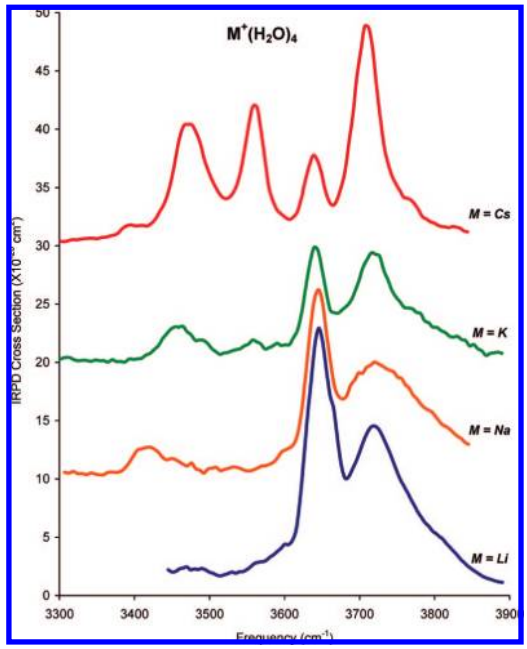

Figure 6. $M^+(H_2O)_4$ IRPD spectra for M = Li, Na, K, and Cs in the free and hydrogen-bonded OH stretching regions.

Thus, the RRKM-EE-estimated temperature for $K^+(H_2O)_4$ is 270 K, 35 K cooler than the temperature calculated for the $Na^+(H_2O)_4$ cluster ion. At 270 K, the minimum-energy K4c isomer contains a linear hydrogen bond. A non-hydrogen-bonded isomer (K4d) and an isomer containing bent water···water hydrogen bonding (K4a) are ~7 kJ/mol higher in energy. From the IRPD spectrum of $K^+(H_2O)_4$, each of these low-lying isomers is present. However, the weak IR intensity of the hydrogen-bonded features relative to the symmetric stretch (3640 cm^{-1}) indicates that the majority of the $K^+(H_2O)_4$ isomers do not contain water···water interactions.

In the $Cs^+(H_2O)_4$ spectrum the intensity of both the convoluted bent/cyclic-trimer hydrogen-bonded transition (3560 cm^{-1}) and the linear hydrogen-bonded transition (3473 cm^{-1}) increases relative to the symmetric OH stretch (3638 cm^{-1}). This suggests that now the majority of $Cs^+(H_2O)_4$ isomers have some type of water···water hydrogen bonding. As depicted in Figure 2, the single-donor hydrogen-bonded water molecules have a second "free" OH oscillator.[32] The vibrational band associated with this mode overlaps somewhat with the asymmetric OH stretch and is responsible for the marked increase in intensity and a narrowing of the transition near 3710 cm^{-1}. Thus, this non-hydrogen-bonded free OH transition is an additional indicator of hydrogen bonding in $Cs^+(H_2O)_4$ clusters.

All of the low-lying structures of $Cs^+(H_2O)_4$ located and shown in Figure 2 contain some type of water···water hydrogen bonding. At the RRKM-EE-estimated temperature for $Cs^+(H_2O)_4$, 275 K, the C4b (containing a cyclic hydrogen-bonded water trimer) and C4d (single linear hydrogen bond) conformations are nearly isoenergetic and the minimum-energy isomers, the latter giving rise to the band at 3473 cm^{-1}, and the former contributes to the feature at 3560 cm^{-1} as mentioned above. It is worth noting that the simultaneous presence of these two hydrogen-bonded bands in the spectrum is only possible with both isomers present in the $Cs^+(H_2O)_4$ cluster ion ensemble. To higher energy, the C4c (5.6 kJ/mol) and C4a (14.3 kJ/mol) isomers are located. The change in free energy with respect to the temperature of the low-lying $Cs^+(H_2O)_4$ isomers is shown in Figure 8. It is unlikely that the isomer with the hydrogen-bonded cyclic water tetramer (C4a) is present in the molecular beam as the remaining low-lying isomers account for the features observed in the $Cs^+(H_2O)_4$ spectrum. Interestingly, this structure, C4a, was the dominant contributor to the $Cs^+(H_2O)_4Ar$ spectrum.[8]

4.5. $M^+(H_2O)_5$. Many different water···water interactions are possible when five water molecules hydrate a cation, including conformations where more than one type of water···water hydrogen bond is present. In isomers with more then one type of hydrogen bonding, the frequency associated with each hydrogen bond is slightly shifted from the hydrogen-bonded frequency in isomers where only one type of hydrogen bond is present. This phenomenon was discussed in the cold $Na^+(H_2O)_5Ar$ and $Li^+(H_2O)_5Ar$ spectra, where different isomers containing similar types of hydrogen bonds were identified by slight shifts in the hydrogen-bonded OH stretching frequencies.[8] In the warmer $M^+(H_2O)_5$ spectra, however, such detail is obscured by the broader OH transitions and prevents experimental identification of specific isomers. Therefore, only general assignments of the observed features to a type of hydrogen-

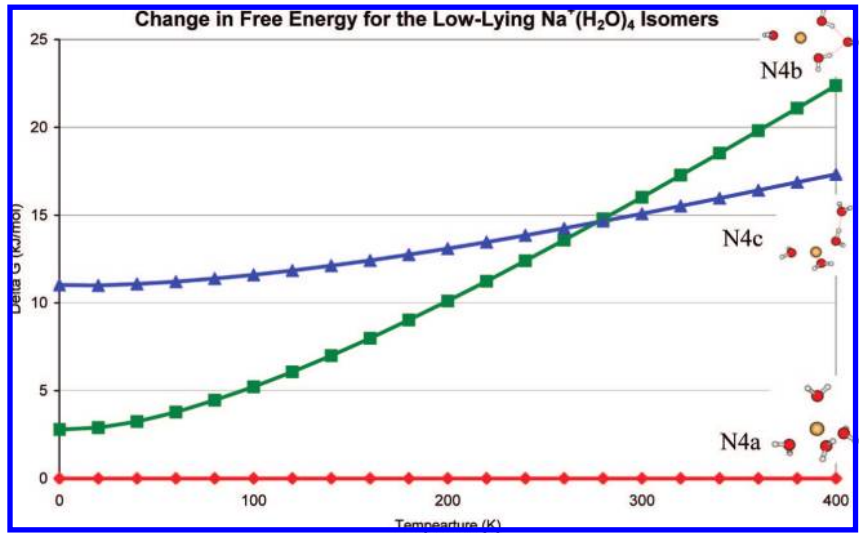

Figure 7. Change in free energy with respect to temperature (0−400 K) for the low-lying $Na^+(H_2O)_4$ isomers: N4a, N4c, N4b.

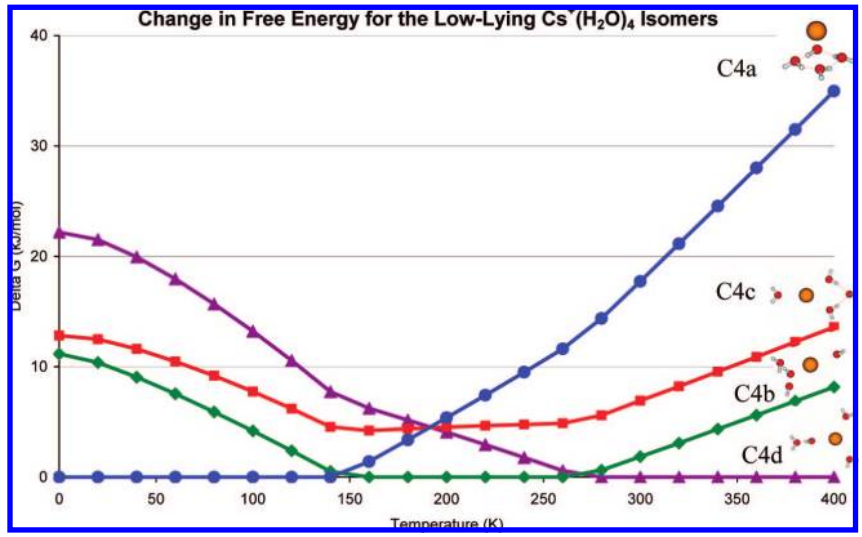

Figure 8. Change in free energy with respect to temperature (0−400 K) for the low-lying $Cs^+(H_2O)_4$ isomers: C4d, C4b, C4c, C4a.

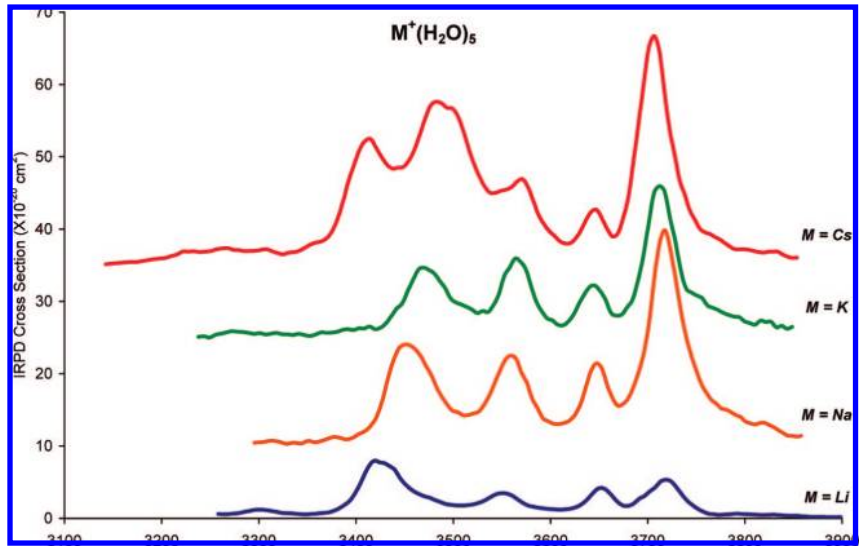

Figure 9. $M^+(H_2O)_5$ IRPD spectra for M = Li, Na, K, and Cs in the free and hydrogen-bonded OH stretching regions.

bonding interaction can be made in these larger, warmer $M^+(H_2O)_5$ cluster ions.

The possible overlapping of similar spectral features from multiple isomers makes each of the $M^+(H_2O)_5$ (M = Li, Na, and K) IRPD spectra, which are shown in Figure 9, appear nearly identical: there are four spectral features, all of which were previously identified in the $K^+(H_2O)_4$ and $Cs^+(H_2O)_{3-4}$ spectra. In the non-hydrogen-bonding region and the symmetric ($\sim$3645 cm^{-1}) and convoluted asymmetric/free OH stretching modes ($\sim$3715 cm^{-1}) are observed. Lower in frequency, in the hydrogen-bonded region, a linear (3430−90 cm^{-1}) and bent hydrogen-bonded feature (3550−70 cm^{-1}) are also observed for each of the $M^+(H_2O)_5$ species.

While little more information may be directly gleaned from the experimental spectra, theoretical analysis of the stable low-lying isomers and the changes in relative energetic ordering as a function of temperature reveals the balance between electrostatic, hydrogen-bonding, and entropic effects that gives rise to the observed spectra. The experimental and theoretical spectra of $K^+(H_2O)_5$ are shown in Figure 10, and the low-lying structures are shown in Figure 2. In Figure 11, the change in free energy as a function of temperature is shown for $K^+(H_2O)_5$; of particular interest is the 250−300 K region, which encompasses the experimental cluster temperature. There are several energetic rearrangements as the temperature increases. A RRKM-EE temperature was not estimated for the larger $M^+(H_2O)_5$ clusters; however, their internal energy content should be similar to those estimates for the $M^+(H_2O)_4$ clusters, which for $K^+(H_2O)_4$ was near 270 K (see Table 3). At this temperature an isomer containing two first-to-second-shell linear hydrogen bonds is the most energetically stable $K^+(H_2O)_5$ configuration. This entropically driven open structure minimizes hindrances on the movement or rotations of the hydrating water molecules. Of the six low-lying $K^+(H_2O)_5$ isomers calculated, five are within 5 kJ/mol of the minimum-energy isomer at 270 K and all are possible contributors to the experimental spectrum. Note that the linear and bent/cyclic hydrogen-bonded OH stretches tend to group together for each of the isomeric species in that the linear bands tend to be below 3500 cm^{-1} while the bent/cyclic ones are between 3500 and 3600 cm^{-1}.

As the electrostatic ion···water interaction strength increases from potassium to lithium, the number of stable low-lying

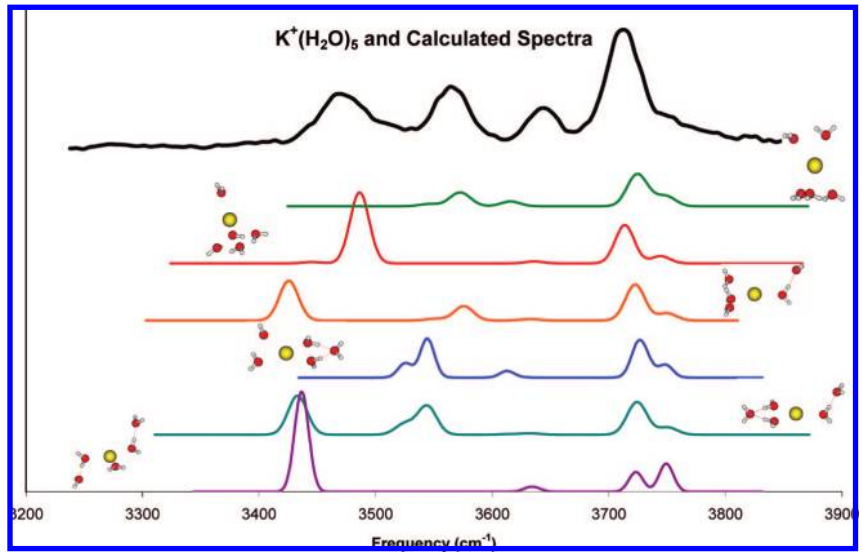

Figure 10. Experimental (top trace) and theoretical spectra (lower traces) of $K^+(H_2O)_5$. Theoretical spectra are ordered based on relative energies at the RRKM-EE-estimated temperatures from most energetically stable to least energetically stable (bottom to top).

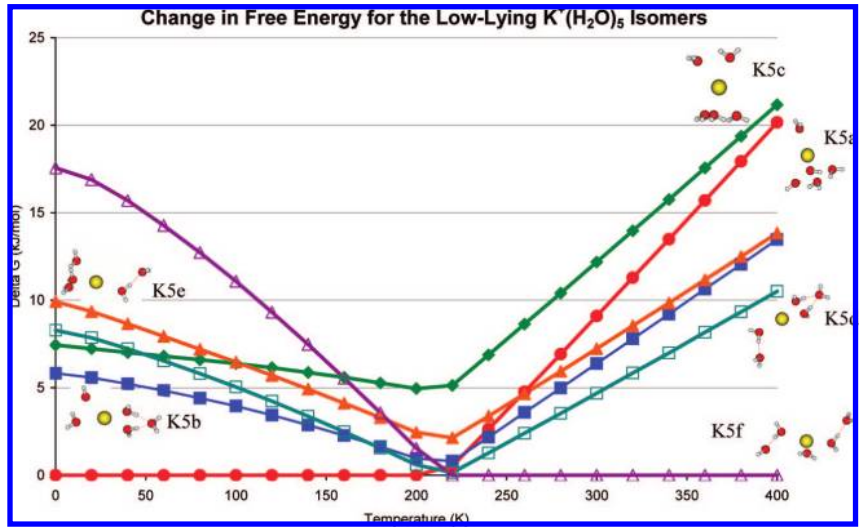

Figure 11. Change in free energy with respect to temperature (0−400 K) for the low-lying $K^+(H_2O)_5$ isomers: K5f, K5d, K5b, K5e, K5a, K5c.

isomers diminishes and the energetic separation between the structures increases. For the $Li^+(H_2O)_5$ cluster, where the strongest ion···water interactions occur, an isomer with all five water molecules in the first solvent shell was located (L5c). A similar structure was not located for either the $Na^+(H_2O)_5$ or the $K^+(H_2O)_5$ cluster. The presence of such an isomer could account for the similar IR intensity of the symmetric and asymmetric/free OH transitions observed in the $Li^+(H_2O)_5$ spectrum.

The $Cs^+(H_2O)_5$ spectrum, shown in Figure 9, has a new hydrogen-bonded OH feature (3410 cm^{-1}) lower in frequency than the previously identified bent/cyclic-trimer hydrogen-bonded feature (3565 cm^{-1}) and the linear hydrogen-bonded feature (3488 cm^{-1}). This suggests that a stronger hydrogen-bonded moiety is present. From the $Cs^+(H_2O)_4$-estimated cluster temperature, the $Cs^+(H_2O)_5$ cluster is expected to be near 275 K, and the change in free energy as a function of temperature for the low-lying $Cs^+(H_2O)_5$ clusters is shown in Figure 12. Near 275 K, the C5b isomer (containing a cyclic hydrogen-bonded water tetramer) is predicted to be nearly isoenergetic with the C5e isomer (bent hydrogen-bonded species), and both isomers are within ∼10.6 kJ/mol of the minimum-energy isomer. Bent hydrogen-bonded features were identified in the smaller $Cs^+(H_2O)_{3-4}$ clusters and in the $M^+(H_2O)_5$ (M = Li, Na, and K) spectra; therefore, this structure is also expected in the $Cs^+(H_2O)_5$ molecular beam, making it energetically plausible that the C5b isomer is also present in the molecular beam. Only cyclic hydrogen-bonded water tetramer and pentamer structures have hydrogen-bonded OH stretches lower in frequency than the linear hydrogen-bonded OH bands (excluding the high-energy C5h structure). The experimental and theoretical spectra of $Cs^+(H_2O)_5$ and the low-lying isomers are shown in Figure 13. There is good agreement between the cyclic hydrogen-bonded features and the new hydrogen-bonded feature near 3410 cm^{-1}, which further supports the assignment of the low-lying hydrogen-bonded feature to cyclic tetramer water···water interactions. Such cyclic water···water interactions were also observed in the $Cs^+(H_2O)_{x\geq 3}Ar$ spectra,[8] where the reduced internal energy allowed such extensive hydrogen-bonded networks to exist.

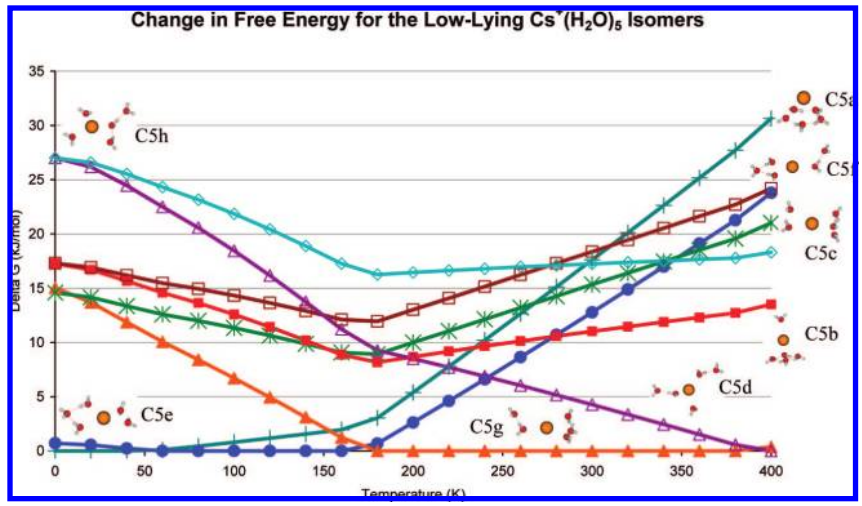

Figure 12. Change in free energy with respect to temperature (0−400 K) for the low-lying $Cs^+(H_2O)_5$ isomers: C5g, C5d, C5b, C5h, C5c, C5e, C5f, C5a.

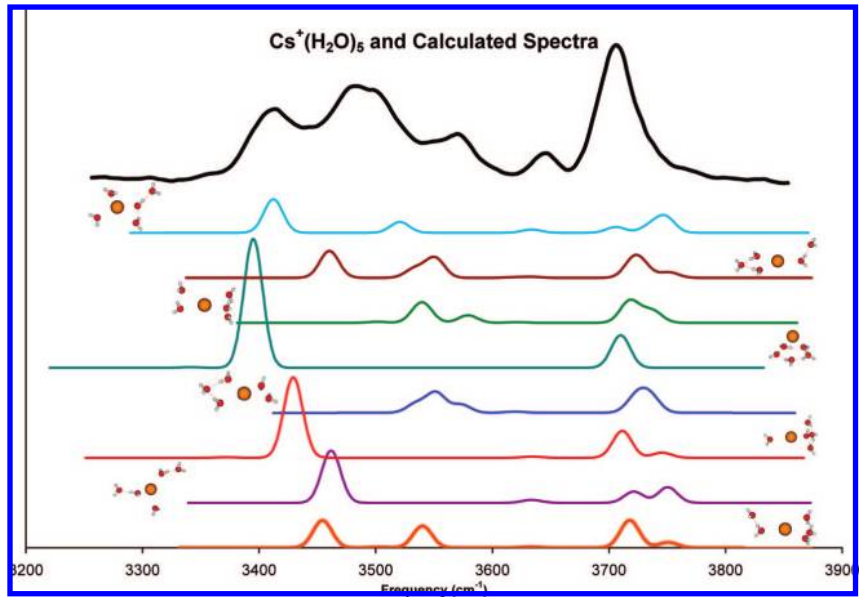

Figure 13. Experimental (top trace) and theoretical spectra (lower traces) of $Cs^+(H_2O)_5$. The theoretical spectra have been offset according to their relative energy ordering based on RRKM-EE-estimated temperatures from the most to least energetically stable (bottom to top).

5. Conclusions

We systematically probed competition and cooperation between noncovalent interactions in $M^+(H_2O)_{2-5}$ cluster ions with elevated internal energies. The observed spectra revealed that extensive water···water hydrogen-bonding interactions were not favored until four or more water molecules were incorporated into the cluster. In all of the $M^+(H_2O)_x$ clusters similar water···water interactions were observed: bent hydrogen bonding (in hydrated cesium clusters, this feature may be convoluted with a cyclic water trimer hydrogen-bonded network) or linear hydrogen bonding. For the smaller Li^+ and Na^+ cations, where electrostatic interactions are the strongest, extensive water···water interactions were observed only after five water molecules were incorporated into the cluster. This is contrasted with the behavior observed in the previously reported cold $Li^+(H_2O)_4Ar$ and $Na^+(H_2O)_4Ar$ spectra, where hydrogen-bonded interactions were prevalent after addition of a fourth water molecule.[8] The onset of extensive water·water hydrogen bonding is a clear indication of the cation coordination number. In the case of the warm $M^+(H_2O)_x$ cluster ions for M = Li, Na, and K, extensive hydrogen bonding occurred at $x = 5$, indicating a gas-phase coordination number of four for these cations. In the $Cs^+(H_2O)_x$ clusters extensive hydrogen bonding is observed by $x = 4$, corresponding to a gas-phase coordination number of three for the cesium cation.

The temperature of the cluster played an important role in determining the observed ion coordination. In the cold $M^+(H_2O)_xAr$ clusters,[8] extensive hydrogen bonding is observed by $x = 3$ for the cesium cation and by $x = 4$ for the remaining cations. In each of these systems this indicates a first-shell occupation number of three (cesium is interacting with a cyclic trimer moiety). Such cyclic structures are less favorable in terms of free energy for the $M^+(H_2O)_x$ systems, where isomers with fewer hydrogen bonds gain entropic stability.

Regardless of the cluster constituents, the RRKM-EE-estimated temperature of the $M^+(H_2O)_x$ cluster ions tended toward 300 K as x increased from $x = 2$ to 5. This suggests that the inherent internal energy content of larger cluster systems that have been cooled by water evaporation will be of similar magnitude independent of the other more strongly bound cluster constituents. This experimental observation supports recent theoretical work suggesting that clusters cooled by water evaporation will tend toward a temperature of 240 K.[61]

Acknowledgment. This material is based on work supported by the National Science Foundation under grant numbers CHE-0415859 and CHE-0072178. Acknowledgment is made to the Donors of the American Chemical Society Petroleum Research Fund for partial support of this research. Earlier measurements on these systems were performed by Dr. Corey J. Weinheimer, Dr. Orlando, and Mr. Cabarcos. Our appreciation is extended to Dr. Timothy Vaden for his experimental and computational assistance.

Supporting Information Available: Complete refs 33 and 35. This material is available free of charge via the Internet at http://pubs.acs.org.

JA803666M

(61) Caleman, C.; van der Spoel, D. *J. Chem. Phys.* **2006**, *125* (15), 154508.